INTERNATIONAL JOURNAL OF AUTOMOTIVE AND MECHANICAL ENGINEERING (IJAME)
ISSN: 2229-8649 e-ISSN: 2180-1606
VOL. 17, ISSUE 3, 8214 – 8223
DOI: https://doi.org/10.15282/ijame.17.3.2020.15.0619

ORIGINAL ARTICLE

Tuft Flow Visualisation on UTM-LST VFE-2 Delta Wing Model Configuration at High Angle of Attacks

M. Said[1*], M. Imai[2], S. Mat[1*], N. Nasir[1], K. A. Kasim[1], N. A. R. Nik Mohd[1] and S. Mansor[1]

[1]Department of Aeronautics, Automotive and Ocean Engineering, School of Mechanical Engineering, Universiti Teknologi Malaysia, Johor Bahru, MALAYSIA
Phone: + 6075535844; Fax: +6075535997
[2]Department of Mechanical Engineering, Tokyo University of Agriculture & Technology, Tokyo, JAPAN

ABSTRACT – This paper reports on flow visualisation and surface pressure measurements over the upper surface of a blunt-edged delta wing model at high angles of attack. The flow structure above the upper surface of the blunt-edged delta wing was found to be different compared to delta wing with sharp leading edge. The flow becomes more complicated especially in the leading edge region of the wing. Currently, there is no data available to verify if the primary vortex could reach the apex of the wing when the angle of attack is further increased. Most prior experiments were performed at the angles of attack, α, below 23° with only a few experiments that had gone to α = 27°. These prior experiments and some CFD works stipulated that the attached flow continue to exist in the apex region of the delta wing even at very high angles of attack above 23°. In order to verify this hypothesis, several experiments at high angles of attack were conducted in Universiti Teknologi Malaysia Low Speed wind Tunnel (UTM–LST), using a specially constructed VFE2 wing model equipped with blunt leading edges. This series of experiments employed two measurement techniques; the first was the long tuft flow visualisation method, followed by surface pressure measurements. The experiments were performed at Reynolds numbers of 1.0×10^6 and 1.5×10^6. During these experiments, several interesting flow characteristics were observed at high angles of attack, mainly that the flow became more sensitive to changes in Reynolds number and the angles of attack of the wing. When the Reynolds number increased from 1×10^6 to 1.5×10^6, the upstream progression of the initial point of the main vortex was relatively delayed compared to the sharp-edged delta wing. The experiments also showed that the flow continued to be attached in the apex region up to α = 27°.

ARTICLE HISTORY
Revised: 10th May 2020
Accepted: 2nd June 2020

KEYWORDS
Delta wing VFE-2;
Flow visualisation;
High angle of attack;
Slender delta wing;
Primary vortex migration

INTRODUCTION

There is always needs to produce delta-wing aircraft that can fly at supersonic speeds. Most of the supersonic transportation (SST) is integrated with delta planform main wing [25]. Delta wing has the advantage of having a small frontal projection area that reduces drag significantly. Most of the delta-winged aircraft were fabricated with its leading-edge profile that is considered blunt, due to requirements of subsonic flight regimes. Many studies on the flow around blunt-edged delta wing have been carried out [1–6]. However, the flow around the wing is very complicated, and it is difficult to solve numerically. More research is needed to verify the complexity of the flow [6].

In order to further investigate the flow of blunt-edged delta wing, a worldwide research group was formed to perform experiments called the Vortex Flow Experiment-2 (VFE-2). The main objective of the VFE-2 tests was to validate the results of Navier-Stokes calculations with experimental data [5, 7]. Figure 1 shows the sample of the results obtained from past VFE-2 campaigns. The experiments in VFE-2 were carried out for both sharp and blunt-edged wings [6, 8]. The results obtained so far were compared with the numerical analysis.

The results show that primary vortex would develop starting at certain chord-wise positions from the wing apex. Upstream from this position to the apex, the flow is attached. The onset point of this primary vortex would move upstream when the angles of attack are increased. The flow over delta wing is very complicated when compared to the conventional wing. When the air passes a delta wing model at a certain angle of attack, the pressure difference between the lower and the upper surface would increase the pressure gradient between the regions, which caused the flow from the lower surface to move to the upper surface in a swirling form called primary vortex. The primary vortex is attached to the surface at a certain range of angles of attack. If the angle of attack is increased, the primary vortex becomes stronger causing it to lift off from the wing surface. The additional vortex lift created at high angles of attack has given significant advantages to delta wings compared to conventional wings [12, 13]. However, the excessive increase of angle of attack induced unsteady flow, and this situation could cause a sudden collapse of the vortex flow, causing the strength to drop. This phenomenon is called vortex breakdown [14] similar to stall conditions on conventional wings. The vortex breakdown can reduce the aircraft longitudinal statics stability and lift force. Many investigations were performed on the vortex breakdown, and the

*CORRESPONDING AUTHOR | M. Said | ✉ mazuriah2@graduate.utm.my

general conclusions are that the characteristics of vortex breakdown depend on wing geometry, Reynolds number and angles of attack [15, 16].

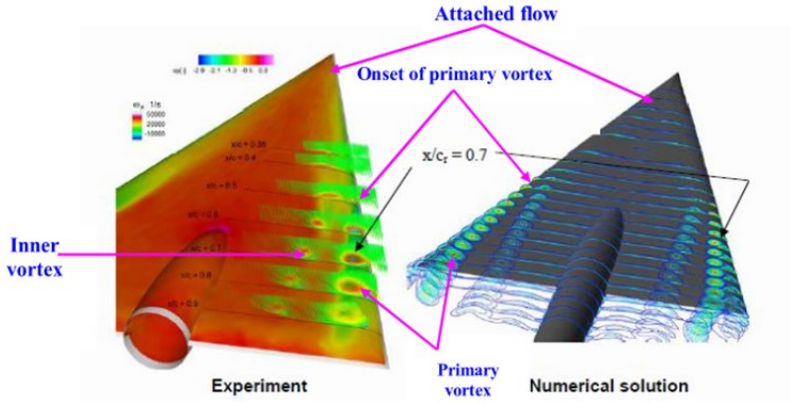

Figure 1. Comparison of experimental measurement and Numerical studies for VFE-2 configurations at α=13° [6, 17].

Many technical data had been published on blunt leading edge VFE-2 profile in the early 2010s [6, 8–11]. The round-edged wing exhibits different flow topology compared to the sharp-edged wing, especially in the region near the leading edge and the apex. The main difference is that for blunt edge wing, there is attached or non-separated flow in the apex region and near the leading edged of the wing. The blunt leading edge weakens the primary vortex, resulting in reduced vortex-induced normal force [6]. This causes the delay of primary vortex appearance; in other words, the vortex starts at positions further down the chord, compared to wing with a sharp leading edge. The flow stays attached to the wing surface from the apex to a certain chord-wise position from which the vortex starts, depending on the Reynolds number, angle of attack, Mach number and how blunt the leading-edge profile itself [22-23].

The flow above a blunt-edged delta wing very much depends upon the Reynolds number. At lower Reynolds numbers the primary vortex develops in the region very close to the wing apex. Many data have shown that the onset of the primary vortex would shift downstream when the Reynolds numbers are increased. This situation happens because of the stronger ability of the turbulent boundary layer, to endure the adverse pressure gradient, to delay the development of vortex further down the chord of the wing when the Reynolds number increased [10]. The flow pattern over the delta wing also depends on the angle of attack. With increasing angles of attack, the adverse pressure gradients on the upper surface of the wing also increase, and this situation leads to the upstream movement of the onset of the outer primary vortex [6].

It can be concluded that the aerodynamics and flow physics for the sharp-edged delta is understood to date [23]. However, the flow visualisation studies on blunt-edged delta wings have discovered many new phenomena which are not fully understood, and thus more experimental explorations are needed. There are only a few studies available [8, 22, 26-27] directly related to these efforts. Mat et al. [8] performed several series of flow visualisations using the surface oil technique on four different types of leading-edges at certain Reynolds number and angle of attack. A sample of the results is shown in Figure 2. At lower angles of attack, the flow in the leading-edge region is fully attached starting from the apex to the trailing edge. Then a pair of primary vortex starts to develop at a certain chord-wise position and progresses upstream with increasing angles of attack. However, there is no data in VFE-2 configurations that indicate the vortex would progress up to the apex region of the wing if the angles of attack is increased [11] further.

Sahin, et al [22] performed cross-flow studies in end-view planes on delta wing to investigate the consequences of vortex bursting and stall phenomena at the high range of angles of attack but with the influence of yaw angle. Most of the experiments were performed at the angles of attack lower than α =23º. As there are no available aerodynamic properties over a delta wing with blunt-edge, such as the primary vortex and vortex breakdown at high angles of attack is available beyond the angles of attack α =23º, this current experimental campaign is initiated. The main objective of this current experiments is to perform flow visualisation experiments and surface pressure measurements at higher angles of attack for the blunt-edged VFE-2 delta wing model.

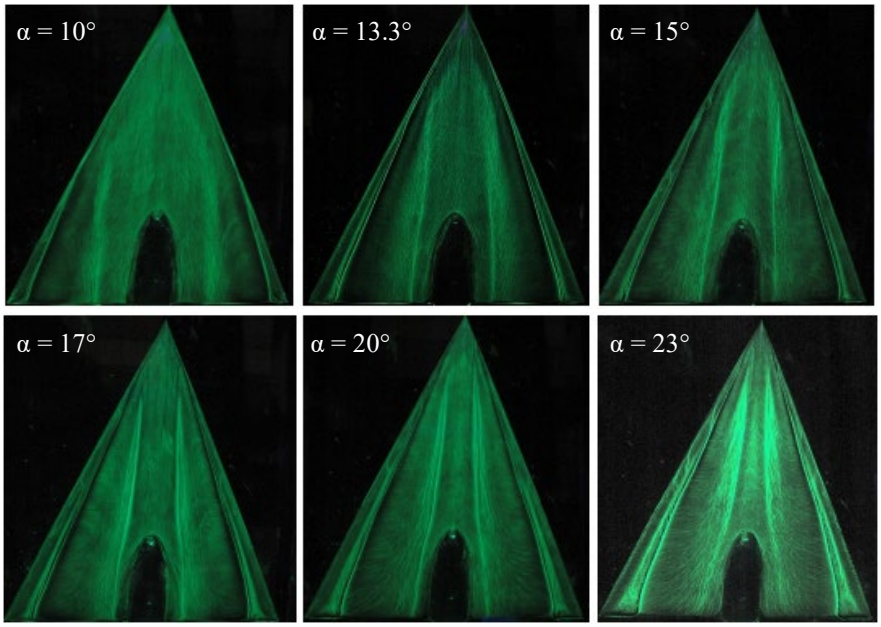

Figure 2. Flow topology above rounded-edged delta wing at Reynolds number of 1×10^6 with α varying from 10° to 23° [8, 17].

METHODOLOGY

The original Vortex Flow Experiment model profile tested as part of the vortex flow experiment campaign 2 (VFE-2) has been replicated and machined again in UTM for further investigations. It has been decided to build a bigger model in UTM compared to the original NASA model in order to obtain higher Reynolds numbers in the subsonic wind tunnel of UTM. The original model has four sets of interchangeable leading edge profiles namely sharp, small-radius, medium-radius and large-radius differentiated by it with a ratio of leading-edge bluntness over maximum wing root chord of $r_{LE/C}$ = 0.0, 0.0005, 0.0015 and 0.0030 respectively. In UTM, an aluminium Alloy 6060 T6 delta wing with two interchangeable leading edges of medium and large-radiuses were fabricated. Figure 3(a) compares the maximum root chord length of the NASA and UTM model. The ratio of leading-edge radii over the wing mean aerodynamic chord were $r_{LE/C}$= 0.0030 for the large and $r_{LE/C}$= 0.0015 for medium-radius wing. The analytical function of the leading edge bluntness over the chord ratio of the wing is shown in Figure 3(c).

Figure 3(c) shows different four sets of leading-edge contour, namely sharp, small, medium and large wing. The contour equation is given by:

$$\varphi(\xi) = \pm x_1\left(a\sqrt{\xi} + b\xi + c\xi^2 + d\xi^3\right) \quad \text{in range of } 0 \le \xi \le 1. \tag{1}$$

To differentiate the leading edge profiles, Chu and Luckring [1– 4] provided the coefficient of *a, b, c*, and *d* as the leading edge coefficients and this is shown in Table 1. Four sets of leading-edge namely sharp, small, medium, and large L.E radii representing the ratios of leading-edge radii to the mean aerodynamic chords of 0, 0.05, 0.15, and 0.3 were fabricated within the VFE-2 campaign. The final assembly of UTM VFE-2 model is shown in Figure 4, while its main dimensions are shown in Table 2. References [1-4] give more details of the leading edge profiles and their analytical definitions.

Table 1. Leading-edge coefficients.

$r/\bar{c}$ (percent)	a	b	c	d
0.00 (sharp)	0.00	3d	-b	0.113338668
0.05 (small)	0.066666667	0.215016	-0.256682667	0.088338667
0.15 (medium)	0.115470053	0.123509650	-0.195678433	0.700373970
0.30 (large)	0.163299316	0.033892978	-0.135891855	0.052101423

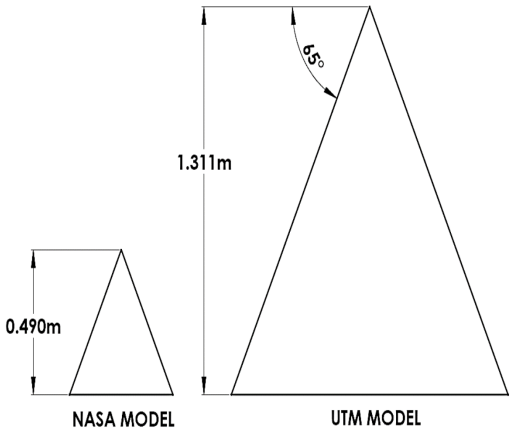

(a) Root chord of NASA and UTM model

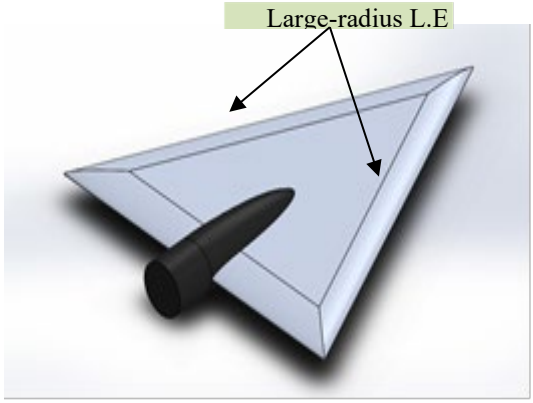

(b) UTM large-radius LE wing

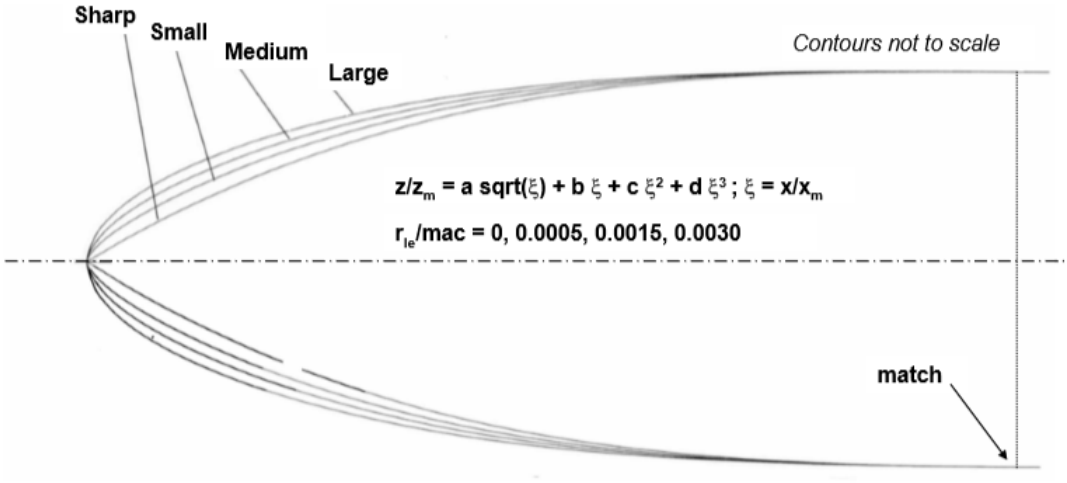

(c) Leading edge contours (from [1–4]).

Figure 3. Delta wing model geometry.

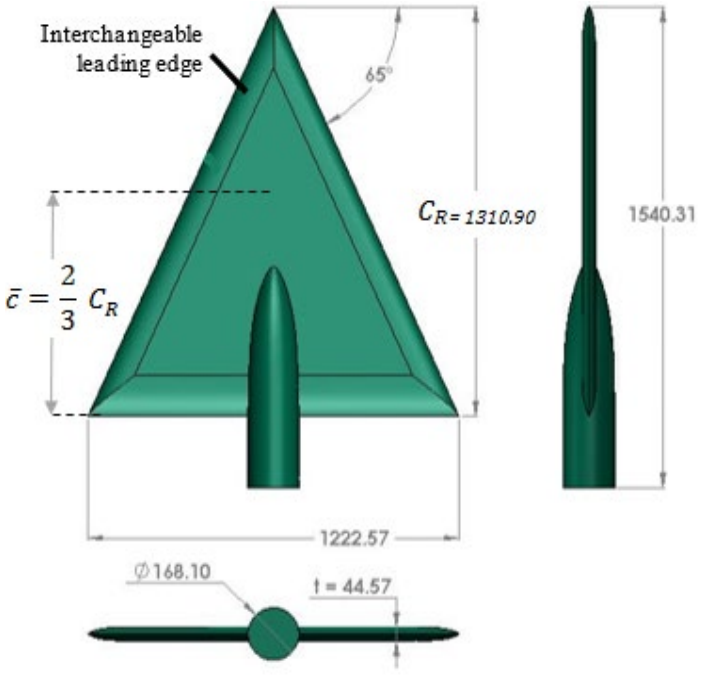

Table 2. UTM VFE-2 delta wing profiles

Dimensions	Values
Root chord (C_R)	1.311 m
Mean aerodynamic chord ($\bar{c}$)	0.874 m
Semi span ($b/2$)	0.611 m
Wing area (A)	0.801 m^2
Sweep angle (Λ)	65°

Figure 4. Geometry of UTM VFE-2 delta wing model.

In this experiment, the model was installed on a 6-axis heavy capacity external balance through a three strut mounting arrangement, in the 1.5 m×2.0 m closed-circuit UTM wind tunnel [28] as shown in Figure 5(a). The maximum speed of this wind tunnel is 80 m/s. The model has been fabricated in three parts: the first is the main body of the delta wing which

is basically a flat-plate with a contoured sharp trailing edge but without the leading edge. This main wing is equipped to accept two pairs interchangeable of leading-edges which are machined such that they represent two different roundness. The wing model also was built with 98 pressure taps located on the starboard side of the upper surface of the wing. The root chord of the model was chosen to be 1.311m giving a mean aerodynamic chord of 0.874 m so that the highest Reynolds number of 4×10^6 could be achieved at a wind speed of 70 m/s based on the aerodynamic chord. The installation of the blunt-edged delta wing model is shown in Figure 5(b).

The flow over a blunt-edge delta wing depends mainly on the angle of attack and Reynolds number. In this campaign, experiments were performed at two speeds of 17.9 and 26.8 m/s corresponding to 1×10^6 and 1.5×10^6 Reynolds numbers and subsonic flow regime with Mach numbers of 0.053 and 0.079. The model angle of attack was varied manually ranging from $\alpha = 0°$ to 27°. During the experiments, the air density (ρ) and air viscosity were 1.17 kg/m^3 and 1.81×10^{-5} kg/(m.s) respectively.

In order to investigate the vortex properties at higher angles of attack, two measurements techniques were employed on the wing. The first one was the tuft method and followed by surface pressure measurements. The flow visualisation techniques discussed by Shen and Pang [18] were followed during the experiments. The details of the experiment test points are shown in Table 3.

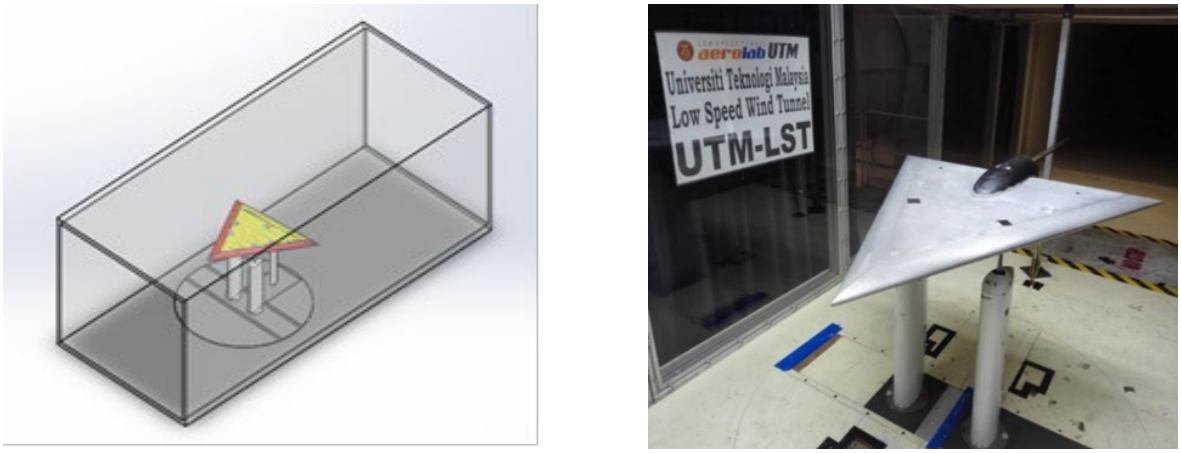

(a) Schematic arrangement of the model in test position in the wind tunnel

(b) Photograph of the installed VFE2 model in the wind tunnel

Figure 5. The installation of UTM VFE-2 model in UTM-LST at $\alpha = 10°$.

Table 3. Experimental conditions.

Reynolds Number, *Re*	1×10^6	1.5×10^6
Velocity, *V* [m/s]	17.9	26.8
Mach Number	0.053	0.079
Angle of attack, α [°]	0, 5, 10, 15, 20, 27	0, 5, 10, 15, 20, 27

Figure 6 shows the tuft experiments in the UTM tunnel. This experiment was conducted using several arrays of threads that had been tied to a grid across the wind tunnel. The length of the threads was 2 m and a total of 600 threads were used, in order to accommodate the size of wind tunnel cross-section which is 2×1.5 m^2. The grid attached with the tufts was then placed in front of the model, such that the free tip of the threads would go past the delta wing model, and as such would capture the aerodynamic flow, including being induced into the vortex over the wing. This method would also provide the sign of the onset of the development of primary vortex, particularly in the leading edge region of the wing [19]. In order to capture and record the behaviour of the strings above the wing, a high-resolution NICON Camera PX was used. The camera was set on its tripod and positioned on the roof of the wind tunnel test section.

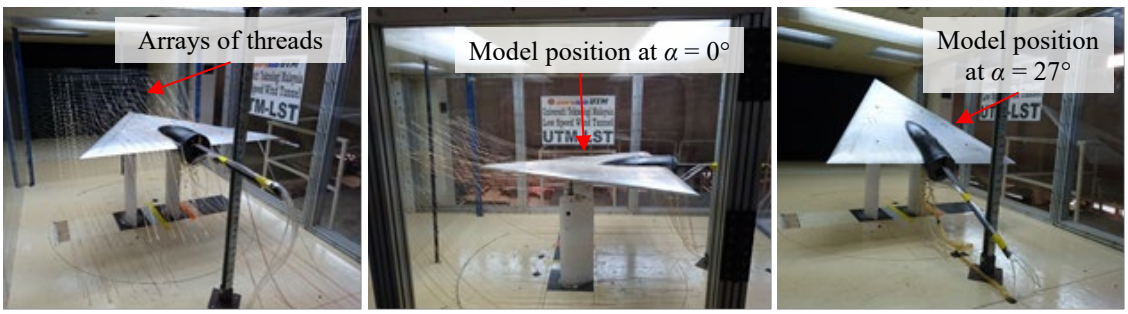

Figure 6. Installation of tufts for flow visualisation experiment.

In order to measure the pressure distribution above the wing, a digitised pressure scanner, as shown in Figure 7 was used. The pressure scanner is the FKPS 30DP Electronic Pressure Scanner with 30 pressure ports. The scanner was connected to a computer such that the pressure readings would be ready tabulated through LabView software. As there were 98 pressure ports on the wing, four pressure campaigns were conducted to gather all 98 pressure points data for each of the two Reynolds numbers (Re = 1×10^6 and Re = 1.5×10^6) and angles of attack from $\alpha = 0^o$ to $\alpha = 27^o$.

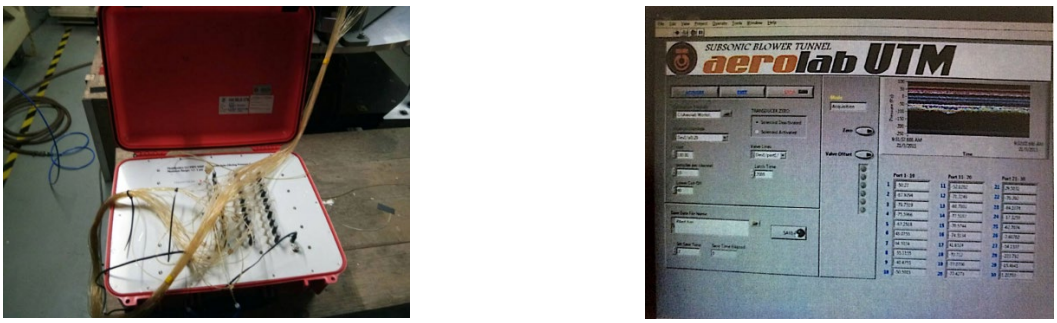

Figure 7. Electronic Pressure Scanner and the computer interphase is giving readings of the pressures.

RESULTS AND DISCUSSION

The images taken from the tuft experiments performed at two Reynolds numbers of 1×10^6 and 1.5×10^6 are shown in Figure 8 and Figure 9, respectively. The photographs show that the formation of the primary vortex, particularly at the leading edge can be detected by this tuft technique. Figure 8 shows that, at zero angle of attack ($\alpha = 0^o$), the flow is fully attached to the wing surface, and the primary vortex is not observed. When the angle of attack was increased to 10^o, a vortex flow was initiated at a certain chordwise position of the wing. Upstream of this point, the flow was still attached to the surface.

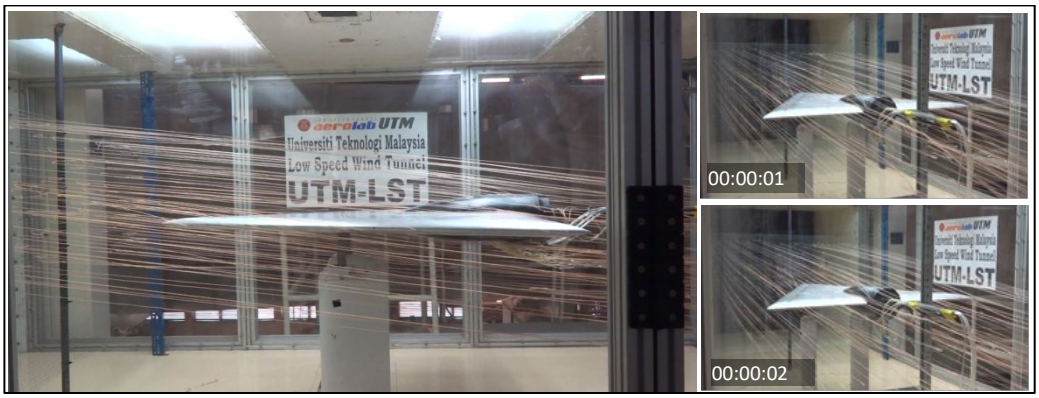

(a) $\alpha = 0^o$ at $Re = 1\times10^6$

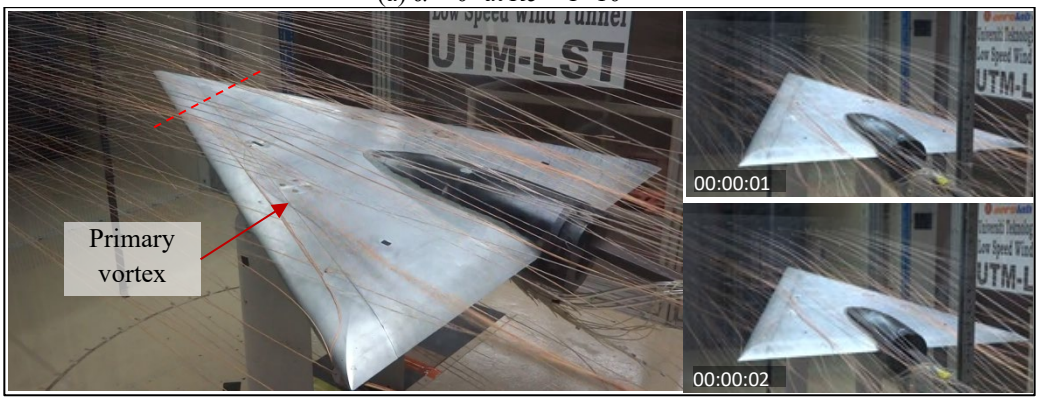

(b) $\alpha = 10^o$ at $Re = 1\times10^6$

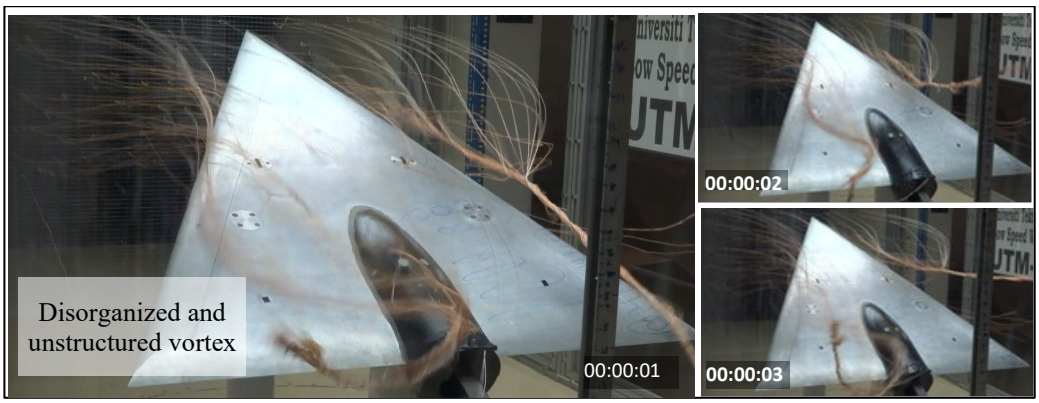

(c) $\alpha = 27^{o}$ at $Re = 1\times10^{6}$

Figure 8. Flow visualisation using long tufts for $Re = 1\times10^{6}$ and angles of attack (a) $\alpha = 0^{o}$, (b) $\alpha = 10^{o}$ and (c) $\alpha = 27^{o}$.

When the angle of attack was increased to the anticipated $\alpha = 27^{o}$, the primary vortex enveloped the entire wing starting from near the apex of the wing. The primary vortex became more significant in size as the flow moved downstream. The main observation at this condition was that the origin of the primary vortex developed very near to the apex of the wing. A closer look onto the apex region showed that the attached flow still existed. However, in the downstream region, the vortex structure has turned into a very disorganised and unstructured pattern. This is where the vortex had broken down. This situation happened for both Reynolds number conditions. It could also be seen that the image for lower Reynolds number condition shows developed vortex compared to the condition for higher Reynolds number. This observation agrees with [20].

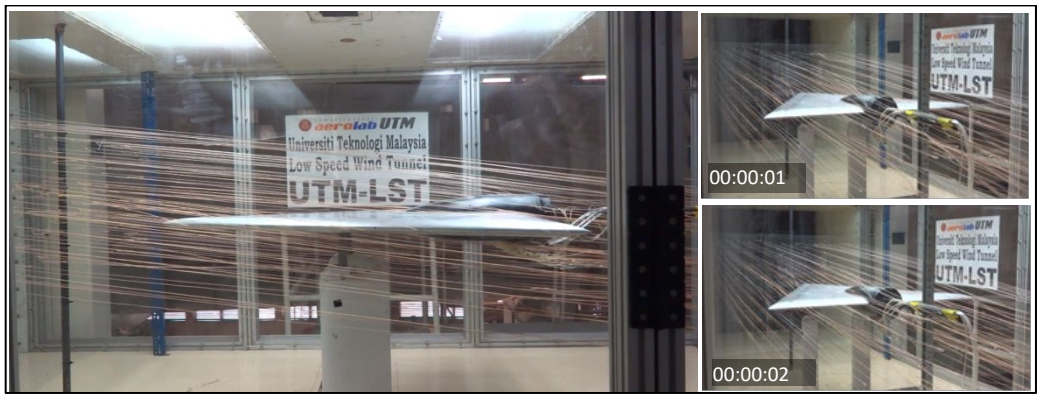

(a) $\alpha = 0^{o}$, Re = 1.5 × 10^{6}

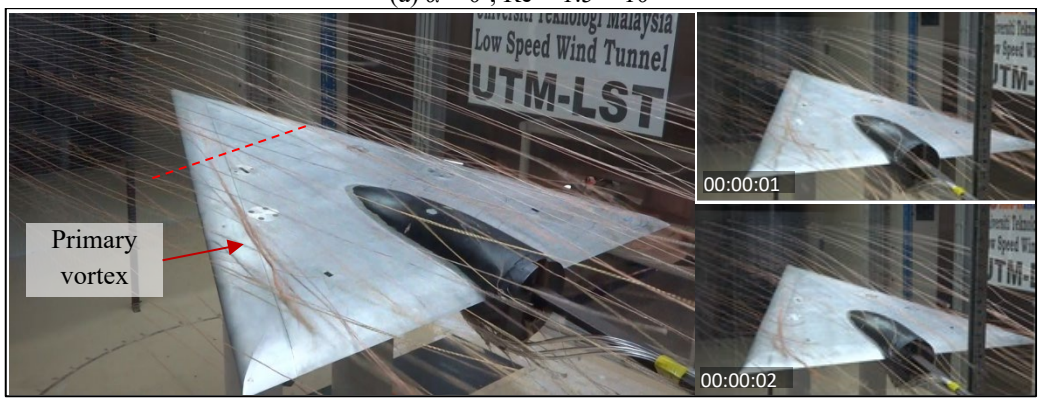

(b) $\alpha = 10^{o}$, Re = 1.5 × 10^{6}

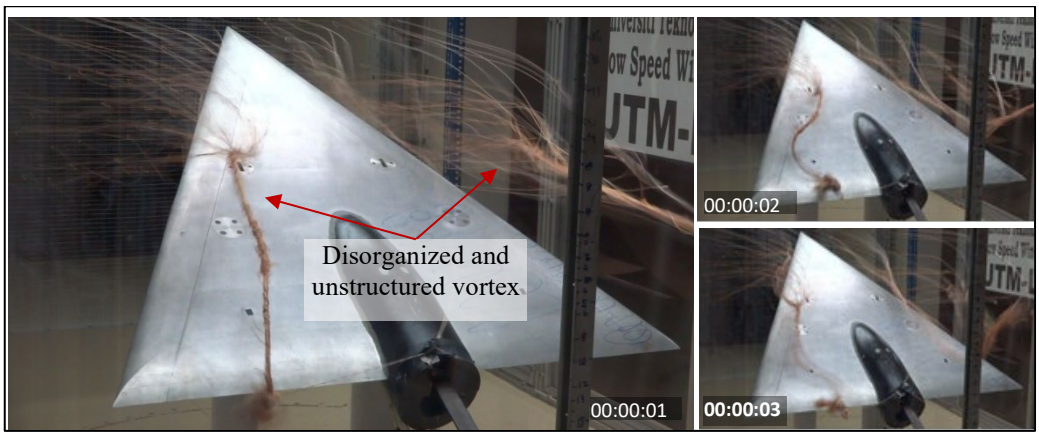

(c) $\alpha = 27^{o}$, Re = 1.5 × 10^6

Figure 9. Flow visualisation using long tufts for $Re = 1.5\times10^6$ and angles of attack of (a) $\alpha = 0^{o}$, (b) $\alpha = 10^{o}$ and (c) $\alpha = 27^{o}$.

The aerodynamic coefficient of lift C_L and drag C_D of the wing model at two different Reynolds number conditions is presented in Figure 10. The figure shows that due to the installation constraints and safety factor, the experiment to measure forces were limited to 25º angle of attack. This emphasised the need to conduct flow visualisation experiment at a high angle of attack, as no force measurement could be conducted above this 25º angle of attack. Overall, the measured forces for the two airspeeds show a similar pattern. The C_L and C_D are relatively higher for the lower Reynolds number flow (Re=1×10^6) particularly at low to moderate angles of attack lower than α = 15°. The higher values of C_L and C_D at lower Reynolds number may be induced by larger separation of the primary vortex in the leading edge.

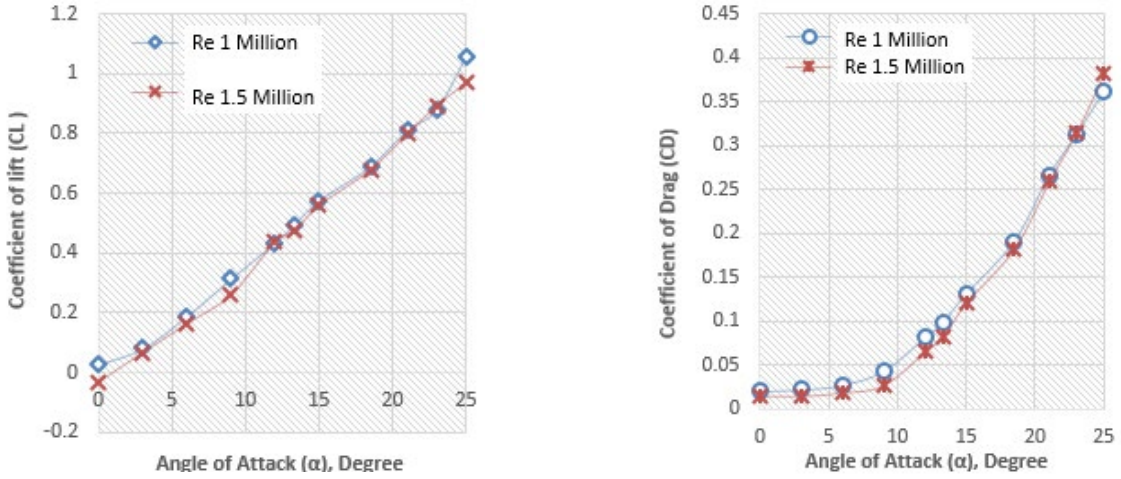

Figure 10. Variations of lift and drag coefficients (C_L and C_D respectively) with angles of attack at $Re = 1.0\times10^6$ and 1.5×10^6.

The effects of the attached flow region are prominent at the Reynolds number of 1.5×10^6 and low angles of attack. The large portion of the attached flow that covers the apex region lowers the C_L and C_D. The results show that the flow characteristics of the delta wing are much influenced by the boundary layer, being either laminar or turbulent. At lower Reynolds number and angles of attack, smooth laminar boundary layer initiates early separation in the leading edge region. At higher Reynolds number, the stronger ability of the turbulent boundary layer to sustain the adverse pressure gradient delays the separation, particularly at lower angles of attack. With increasing angles of attack, the onset of primary vortex moved upstream. At high angles of attack, the upper surface of the wing flow is dominated by the primary vortex even in the apex region.

Figure 11 shows the leading-edge pressures measured at the same time as the flow visualisation experiment. The results supported the observations that in the region near the apex of the wing ($Y/C_r = 0.10$), the flow is completely attached to the wing surface, such that the graph follows the attach flow theory through all angles of attack. Here, Reynolds number did not give much influence to the flow pattern. At $Y/C_r = 0.20$, the flow is still attached, but it has a tendency to separate particularly at lower Reynolds number.

It was also observed, that by increasing the angle of attack, the point of onset of the primary vortex moved upstream. This observation suggested that the flow field of the blunt leading edge will not behave like one on the wing with a sharp edge. But the tuft experiment points toward this forward movement of the onset, but it could not give the full characteristics of the flow in the region. This means there are further needs to employ a more detail flow visualisation techniques to fully understand the flow characteristics.

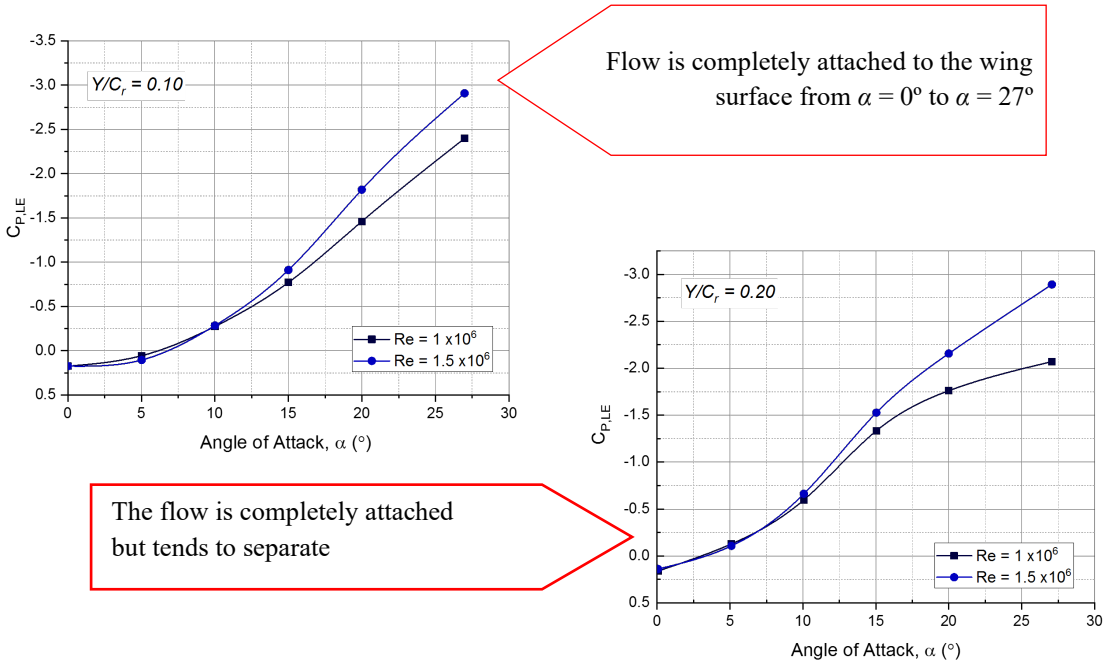

Figure 11. Leading-edge pressures near the apex region.

Due to the limitation of the access area in the apex region, it is very difficult to install enough static pressure holes to allow a comprehensive measurement of on-surface pressures. It would be valuable if other flow visualisation techniques can be employed to provide further information on off-surface flow and nature of the vortices at this targeted area. Further discussion on the flow visualisation techniques can be found in [17, 21, 22]. As for this tuft visualisation method, it is recommended to use more fine strings to obtain better observations.

CONCLUSION

The early result obtained here has pointed that there is attached flow developed in the apex region of the delta wing, even at higher angles of attack. This means that there still exists leading-edge pressures that allow the attached flow to happen. The results emphasise that the primary vortex of the blunt-edge wing will not behave as the sharp-edged wing even when the angle of attack was increased to $\alpha = 27°$ and even higher. It is recommended that more experiments be conducted with several different methods of flow visualisation to verify this result. The experiments at higher than $\alpha = 27º$ also should be conducted to confirm this hypothesis.

ACKNOWLEDGEMENT

This research was funded by grants from Universiti Teknologi Malaysia (21H05, 18H06 & 4Y225). The experiments have been carried out at the Aeronautics Laboratory, Universiti Teknologi Malaysia (Aerolab UTM). The data presented, the statements made and views expressed are solely the responsibility of the authors.

REFERENCES

[1] Chu J, Luckring JM. Experimental surface ressure data obtained on 65° delta wing across Reynolds Number and Mach Number ranges Volume 4 — Large-Radius Leading Edge. NASA Technical Memorandum 4645; 1996.
[2] Chu J, Luckring JM. Experimental surface ressure data obtained on 65° delta wing across Reynolds Number and Mach Number ranges Volume 2 — Medium-Radius Edge. NASA Technical Memorandum 4645; 1996.
[3] Chu J, Luckring JM. Experimental surface ressure data obtained on 65° delta wing across Reynolds Number and Mach Number ranges Volume 1 — Sharp Leading Edge. NASA Technical Memorandum 4645; 1996.
[4] Chu J, Luckring JM. Experimental surface ressure data obtained on 65° delta wing across Reynolds Number and Mach Number ranges Volume 3 — Medium-Radius Leading Edge. NASA Technical Memorandum 4645; 1996.
[5] Hummel DJ. The international vortex flow experiment 2 (VFE-2): Background, objectives and organisation. Aerospace Science and Technology 2013; 24(1):1-9.
[6] Luckring JM, Hummel D. What was learned from the new VFE-2 experiments. Aerospace Science and Technology 2013; 24(1): 77–88.
[7] Luckring JM. Initial experiments and analysis of blunt-edge vortex flows for VFE-2 configurations at NASA Langley, USA. Aerospace Science and Technology 2013; 24(1): 10–21.
[8] Mat S Bin, Green R, Galbraith R, Coton F. The effect of edge profile on delta wing flow. Proceedings of the Institution of Mechanical Engineers, Part G: Journal of Aerospace Engineering, 2015; 230(7): 1252–1262.
[9] Konrath R, Klein C, Schröder A. PSP and PIV investigations on the VFE-2 configuration in sub- and transonic flow. Aerospace Science and Technology 2013; 24(1): 22–31.

[10] Fritz W. Numerical simulation of the peculiar subsonic flow-field about the VFE-2 delta wing with rounded leading edge. Aerospace Science and Technology, 2013; 24(1): 45–55.
[11] Said M, Mat S, Mansor S, Abdul-Latif A, Lazim TM. Reynolds Number effects on flow topology above blunt-edge delta wing VFE-2 configurations. In: 53rd AIAA Aerospace Science Meeting, pp. 1–15; 2015.
[12] Kulfan RM. Wing airfoil shape effects on the development of leading-edge vortices. AIAA Conference on Atmospheric Flight Mechanics for Future Space System, 1979; 79-1675.
[13] Kok J, Fuchs M, Mockett C. Delta wing at high angle of attack. In: Mockett C, Haase W, Schwamborn D, editors. Go4Hybrid: Grey area mitigation for hybrid RANS-LES methods, notes on numerical fluid mechanics and multidisciplinary design 134, 2018, p139–153.
[14] Robertson ED, Chitta V, Walters DK, Bhushan S. On the vortex breakdown phenomenon in high angle of attack. In: ASME 2014 International Mechanical Engineering Congress and Exposition IMECE2014, Montreal, Canada, 1– 9; 2014.
[15] Lucca-Negro O, O'Doherty T. Vortex breakdown: A review. Progress In Energy and Combustion Science, 2001; 27(4): 431–481.
[16] Sidorenko AA, Budovskiy AD, Maslov AA, Postnikov BV, Zanin BY, Ilya DZ, Kozlov VV. Plasma control of vortex flow on a delta wing at high angles. Experiments in Fluids, 2013; 54:1585: 1–12.
[17] Mat SB. The analysis of flow on round-edged delta wings. Retrieved from http://theses.gla.ac.uk/2387/; 23 Feb 2011.
[18] Shen W, Pang A. Tuft flow visualisation. Proceedings of the Second IASTED International Conference on Visualization, Image, and Image Processing, 2002; 2002: 705–710.
[19] Tajuddin N, Mat S, Said M, Mansor S. Flow characteristic of blunt- edged delta wing at high angle of attack. Journal of Advanced Research in Fluid Mechanics and Thermal Sciences, 2017; 39(1): 17 - 25.
[20] Said M, Mat S. Effects of reynolds number on the onset of leading edge vortex separation above blunt-edge delta wing VFE-2 configurations. In: 30th Congress of the International Council of the Aeronautical Sciences, ICAS 2016, Daejeon, South Korea, 2016_0608; 2016.
[21] Htun YE, Yar ZAY, Myint MYO. Some principles of flow visualisation techniques in wind tunnel. International Journal of Advances in Science Engineering and Technology, 2016; 4(2): 62–66.
[22] Sahin B, Oguz Tasci M, Karasu I, Akilli H. Flow structures in end-view plane of slender delta wing. EPJ Web of Conferences, 2017; 143: 02099.
[23] Luckring JM. The discovery and prediction of vortex flow aerodynamics. The Aeronautical Journal, 2019; 729–804.
[24] Said M, Mat S, Mansor S, Ali A. Effects of leading edge enlargement on the primary vortex of blunt-edged delta wing VFE-2 Profile. Acta Polytechnica Hungarica, 2018; 15(8).
[25] Luckring JM. Introduction to the special section on F-16XL flight aerodynamics predictions at a high angle of attack. AIAA Journal of Aircraft, 2017; 54(6): 2013.
[26] Yayla S, Canpolat C, Sahin B, Akilli, H. The effect of angle of attack on the flow structure over the non slender lambda wing. Aerospace Science and Technology, 2013; 28: 417-430.
[27] Wang JJ, Zhang W. Experimental investigations on leading-edge vortex structures for flow over non-slender delta wings. Chinese Physics Letters, 2008; 25(7): 2550.
[28] Noor AM, Mansor S. Measuring aerodynamic characteristics using high performance low speed wind tunnel at Universiti Teknologi Malaysia. Journal of Applied Mechanical Engineering, 2013; 3(1): 1000132.